REAL-TIME CHEMICAL IMAGING OF FUNCTIONAL MATERIALS AND DEVICES: CATALYTIC REACTORS, FUEL CELLS AND BATTERIES

A. Vamvakeros[1,2,3*], D. Matras[4,5], S. D. M. Jacques[2*], M. Di Michiel[3], V. Middelkoop[6], A. M. Beale[1,2,4*]

[1]Department of Chemistry, University College London, 20 Gordon Street, London WC1H 0AJ, UK.
[2]Finden Limited, Harwell Science and Innovation Campus, Harwell, UK.
[3]ESRF – The European Synchrotron, 71 Avenue des Martyrs, 38000 Grenoble, France.
[4]Research Complex at Harwell, Harwell Science and Innovation Campus, Rutherford Appleton Laboratory, Didcot, Oxon, OX11 0FA, UK
[5]School of Materials, University of Manchester, Manchester, Lancashire M13 9PL, UK.
[6]Flemish Institute for Technological Research, VITO NV, Boeretang 200, Mol, Belgium.
(*antony@finden.co.uk, simon@finden.co.uk, andrew.beale@ucl.ac.uk)

ABSTRACT

Supported solid catalysts and functional devices like fuel cells and batteries usually comprise of complex structures exhibiting various heterogeneities which have direct impact on their performance. In order to design novel materials with enhanced properties, it is essential to gain a better understanding of how these heterogeneities are linked to their performance. Synchrotron X-ray based chemical tomography techniques have shown to provide such information; these techniques allow for non-destructive investigation of intact reactors and devices and for extraction of spatially-resolved signals containing physico-chemical information. In this work, we present recent examples where synchrotron X-ray diffraction computed tomography has been employed to study a catalytic reactor and a solid oxide fuel cell under various operating conditions.

INTRODUCTION

Catalytic solids, fuel cells and batteries are functional materials and devices which tend to possess complex heterogeneous structures that often evolve under working conditions [1-3]. As such, it is crucial to characterise these materials systems in situ and indeed operando with non-destructive techniques as gaining a better understanding of the structure-function relationships is crucial in designing new materials with improved properties (e.g. activity, stability and selectivity) [4-7]. In the past decade, there has been a lot of effort from several research groups in developing advanced characterisation techniques that can deliver this requirement. These techniques are typically employed at third generation synchrotrons taking advantage of the brilliant X-rays generated at these large scale facilities. Of particular interest are the chemical tomography techniques where a scattering or spectroscopic technique is combined with the computed tomography data acquisition method yielding spatially-resolved physico-chemical information. X-ray diffraction computed tomography (XRD-CT) is such a technique and it can be used to study different materials systems and devices, varying from catalytic reactors to electrochemical energy devices [8-13].

METHODOLOGY

Catalytic reactor for the partial oxidation of methane reaction

XRD-CT measurements were performed at beamline station ID31 of the ESRF using a 70 keV monochromatic X-ray beam focused to have a spot size of 25 μm x 25 μm. 2D powder diffraction patterns were collected using the Pilatus3 X CdTe 2M hybrid photon counting area detector. The total acquisition time per point was 15 ms (exposure time of 11 ms and readout time of 4 ms) using the continuous rotation/translation data acquisition strategy [14]. Four 3D-XRD-CT scans of the Ni – Pd/CeO2 – ZrO2/Al2O3 catalyst were acquired at different operating conditions: 1) at room temperature, 2) at 800 °C under He flow, 3) at 800 °C under 20 % H2/He flow (reduction step) and

4) at 800 °C under 20 % O2/He flow (oxidation step). Each 3D-XRD-CT scan composed of 30 XRD-CT scans, each one collected at a different vertical position (i.e. with 25 μm step size along the catalyst bed). Each XRD-CT scan lasted approximately 2 min. The tomographic measurements were made with 100 translation steps (translation step size of 25 μm) covering 0 – 180 ° angular range, in steps of 2.5 ° (i.e. 72 line scans). The detector calibration was performed using a CeO2 NIST standard. Every 2D diffraction image was converted to a 1D powder diffraction pattern after applying an trimmed mean filter to remove outliers using in-house developed MATLAB scripts, the nDTomo and pyFAI software packages [15]. The data integration was performed with fast GPU processing [16]. The final XRD-CT images (i.e. reconstructed data volume) were reconstructed using the filtered back projection algorithm. Rietveld analysis of the diffraction data was performed with Topas v5 [17].

Solid Oxide Fuel Cell

XRD-XRD-CT measurements were made at the beamline station ID15A of the ESRF using a 90 keV monochromatic X-ray beam focused to a spot size of 40 μm x 20 μm (Horizontal × Vertical). 2D powder diffraction patterns were collected using the Dectris Pilatus3 X CdTe 2M hybrid photon counting area detector. The total acquisition time per point was 20 ms and each XRD-CT scan lasted in total for 26 min. Initially, an XRD-CT scan was performed at the middle of the SOFC at ambient conditions. The XRD-CT scan consisted of 351 translation steps (translation step size of 20 μm) covering 0 – 180 ° angular range, in 176 steps. Calibration and data processing was carried as described in the section above.

RESULTS & DISCUSSION

Five-dimensional tomographic diffraction imaging of a catalyst bed

The partial oxidation of methane (POX) reaction provides an alternative route to produce H_2 and CO, also known as “synthesis gas” compared to the conventional energy-demanding steam reforming reaction [18]. It is a mildly exothermic reaction and importantly the produced H2:CO molar ratio is equal to 2. This makes it a promising reaction for industrial applications as the outlet stream could be directly fed into Fischer-Tropsch reactors in gas-to-liquids (GTL) plants for the production of synthetic fuels. Similarly to most methane reforming/processing reactions, Ni/Al_2O_3-based solid catalysts have been the most often investigated catalysts for the POX reaction. However, this family of catalysts are usually prone to fast deactivation under POX reaction conditions and this has been attributed to numerous reasons varying from the deactivation of the Ni active sites due to carbon deposition, to Ni particles sintering and even to the occurrence of undesired solid-state reactions in the catalyst bodies such as the formation of the $NiAl_2O_4$ phase [19]. To overcome these stability issues, various different approaches have been explored over the past few decades with two major ones being a) the modification of the Al_2O_3 support and b) the addition of promoters. The latter typically involves the addition of small amounts of a noble metal to the catalyst (e.g. Pd, Pt, Rh and Ru) while the former approach focuses on modifying the Al_2O_3 support through the addition of other components which can provide improved stability of the catalyst. The solid-state solution of CeO_2-ZrO_2 is well-known for its excellent oxygen storage capacity and redox properties. However, these mutli-component systems are rarely studied in situ which limits our understanding of the state of the activated and real working catalyst and the role of each individual component. Synchrotron chemical tomography techniques are emerging as the tools that can provide this crucial type of information. For example, we recently investigated a complex multi-component 10 wt. % Ni – 0.2 wt. % Pd/ 10 wt. % CeO_2 – ZrO_2/ Al_2O_3 catalyst with synchrotron 3D-XRD-CT and showed that it is possible to capture the activated catalyst in 3D and gain a better insight into the various roles of each catalyst component by studying the behaviour of the catalyst under different operating conditions [11].

As shown in Figure 1, the Rietveld analysis of the 3D-XRD-CT data of the fresh catalyst bed provided multi-length scale spatially-resolved physico-chemical information. Specifically, the phase distribution volumes (information at the μm-to-mm level) revealed that only the distribution of Al_2O_3 is homogeneous over the catalyst particles while ZrO_2 exhibits an egg-shell distribution. PdO is predominantly present near the surface of the catalyst particles but it can be seen that it is not well-dispersed (hotspots of this material). The distribution of NiO, albeit present in all particles, is also seen to vary between different catalyst particles. Importantly, the Rietveld analysis of the diffraction data allowed us to estimate the crystallite size (information at the nm level) and the lattice parameters (information at the Å level) of various catalyst components. The combination of this multi-length scale information allowed us to reveal the presence of four distinct CeO_2-ZrO_2 species present in the catalyst:

- A $Ce_xZr_yO_2$ (x>>y) phase with small crystallites present near the surface of the catalyst particles
- A relatively pure CeO_2 phase with larger crystallites closer to the core of the catalyst particles
- A $Ce_xZr_yO_2$ (x<<y) phase with small crystallites near the surface of the catalyst particles
- A relatively pure ZrO_2 phase with larger crystallites near the surface of the catalyst particles (hotspots of this material)

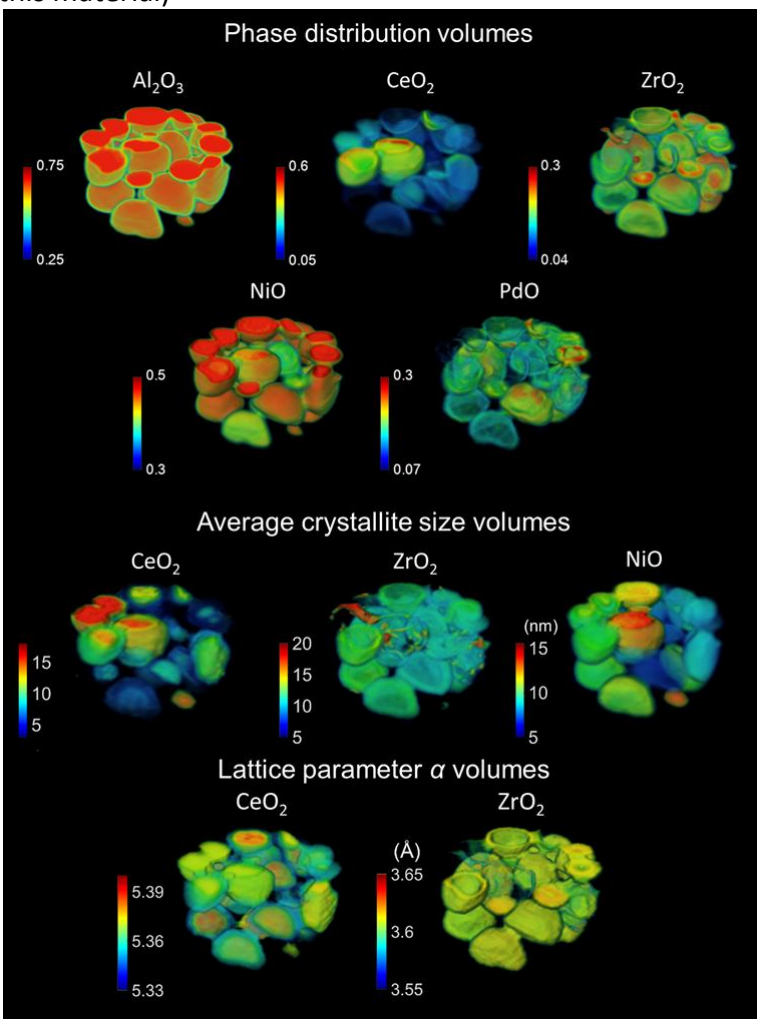

Figure 1. *3D maps obtained from the Rietveld analysis of the 3D-XRD-CT data collected at room temperature. Top: Volume rendering of the normalised scale factors data volume (phase distribution volumes). The values in the colorbar axes have been chosen to achieve the best possible contrast. Middle: Volume rendering of the average crystallite size maps of CeO_2, ZrO_2 and NiO (colorbar axes in nm). Bottom: Volume rendering of the lattice parameter a of CeO_2 and ZrO_2 unit cells (colorbar axes in Å). Figure reproduced from* [11].

It should be noted though that this was the first 5D tomographic diffraction imaging study (i.e. 3D spatial, 1D scattering and 1D to denote time/imposed state) as we were able to study this complex catalyst system in 3D and under different operating conditions. For example, as shown in Figure 2, it was possible to track the evolution of the Ni-containing species in 3D during a reduction-oxidation (redox) experiment. As an example, it was shown that $NiAl_2O_4$ forms during the initial temperature ramp to 800 °C under He and that this phase was more difficult to reduce compared to NiO during the reduction/catalyst activation step. It was also shown that the oxidation step led to the sintering of the Ni species and the presence of larger NiO crystallites showing that the catalyst pre-treatment protocols also play an important role in yielding a catalyst with the desired physical and chemical properties.

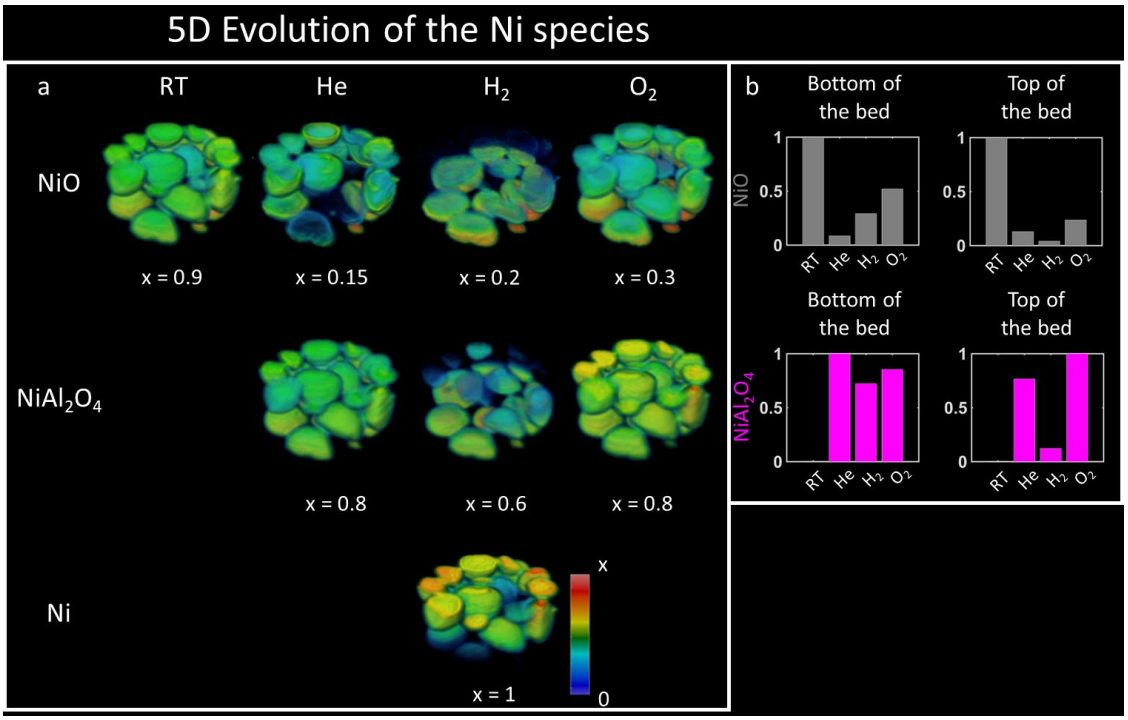

Figure 2. *Phase distribution volumes of NiO, $NiAl_2O_4$ and Ni as obtained from the Rietveld analysis of the 3D-XRD-CT data collected at the four different operating conditions. The values in the colorbar axes have been chosen to achieve the best possible contrast. Figure reproduced from* [11].

Diffraction imaging of a solid oxide fuel cell

We recently also performed the first XRD-CT study of a real life size micro-tubular solid oxide fuel cell (SOFC) [13]. Specifically, the mechanical and structural stability of a state-of-the-art "micro-monolithic" SOFC was investigated with synchrotron XRD-CT during a thermal cycling test. As shown in Figure 3, the Rietveld analysis of the diffraction data allowed us to map the various components present in this electrochemical cell: the NiO-YSZ anode, the YSZ solid electrolyte and the $La_{1-x}Sr_xMnO_3$ (LSM) cathode. It was also possible to map the wt. % of each phase, including a minor SrO phase (<5 wt. %).

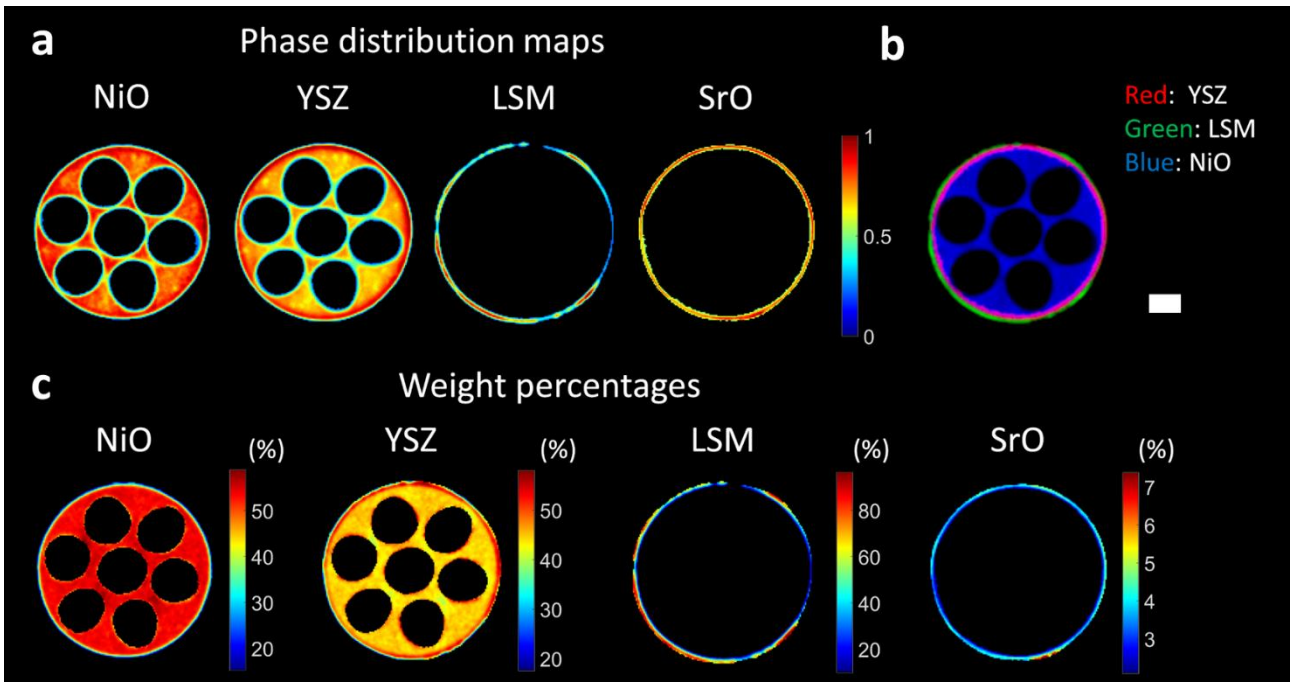

Figure 3. *XRD-CT results from the fresh SOFC. a the phase distribution maps of NiO, YSZ, LSM and SrO as derived from the Rietveld analysis of the fresh SOFC XRD-CT datasets (color bar indicates intensity in arbitrary units), b RGB image showing the distribution of YSZ (red), LSM (green) and NiO (blue), c weight % of all crystalline phases present in the SOFC. The scale bar corresponds to 0.5 mm. Figure reproduced from* [13].

The SOFC was first activated under the flow of H_2 in order to reduce the NiO to the electrochemically active metallic Ni phase and then a thermal cycling test was performed in order to evaluate its mechanical robustness and structural integrity. The results, presented in Figure 4, showed that the cell exhibits excellent stability as the Ni lattice parameter and strain remained consistent for the duration of the experiment.

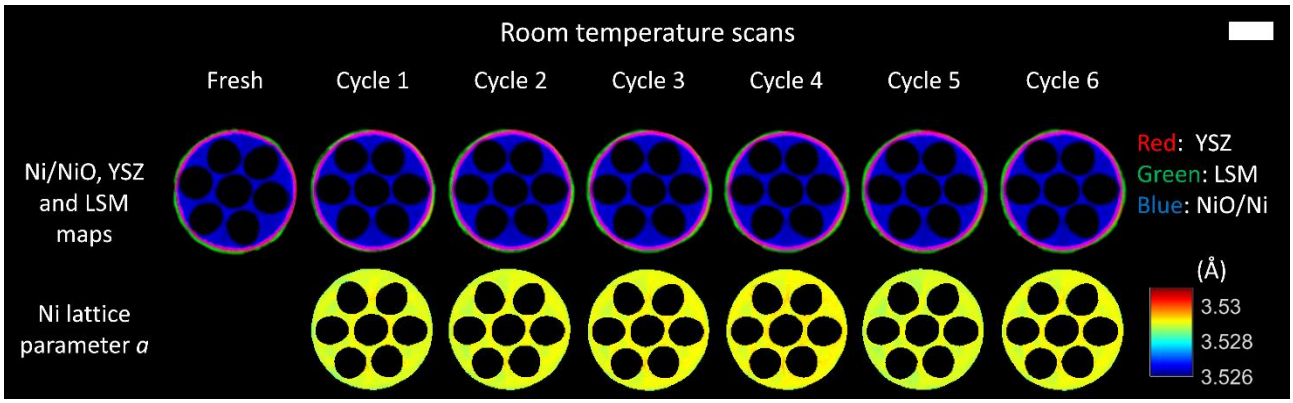

Figure 4. *XRD-CT results obtained during the thermal cycling of the SOFC. Row 1: RGB images showing the distribution of the main SOFC components during the thermal cycling test (red: YSZ, green: LSM and blue: NiO/Ni). Row 2: the Ni unit cell lattice parameter a maps during the thermal cycling test as derived from the Rietveld analysis of the corresponding XRD-CT data. The scale bar corresponds to 0.5 mm. Figure reproduced from* [13].

CONCLUSIONS

Synchrotron X-ray chemical tomographic techniques are state-of-the-art methods that can be applied to investigate complex materials systems non-destructively and extract local physico-chemical information across multiple length scales. We demonstrated this by examining a multi-component Ni-Pd/CeO_2-ZrO_2/Al_2O_3 catalyst under different operating conditions and were able

show that it is possible to correlate the inter and intra-particle gradients in solid-state chemistry with the chemical environment the catalyst particles experience. We also employed synchrotron XRD-CT to investigate the mechanical performance of a new "micro-monolithic" SOFC during a thermal cycling test showing that chemical tomography techniques can be used to study functional materials and devices in general. With the advancements in synchrotron brightness (e.g. upgrades of third generation synchrotrons), detector performance (development of faster and essentially noise-free detectors), sample environment (new reactor cells) and data analysis (e.g. Rietveld analysis of XRD-CT data), X-ray chemical tomography techniques are bound to become increasingly easier to perform and one can readily foresee that they will replace conventional in situ XRD and X-ray imaging as the preferred method for characterising functional materials and devices (e.g. catalytic reactors, batteries and fuel cells).

ACKNOWLEDGMENTS

The authors would like to thank the ESRF for beamtime. Antonis Vamvakeros and Dorota Matras acknowledge the research funding provided by the European Union Horizon 2020 research and innovation programme under Grant Agreement No. 679933 (MEMERE project).

REFERENCES

[1] A.M. Beale, S.D. Jacques, B.M. Weckhuysen. Chem. Soc. Rev. 39 (12) (2010) 4656-72.
[2] J.D. Grunwaldt, C.G. Schroer. Chem. Soc. Rev. 39 (12) (2010) 4741-53.
[3] J. Nelson Weker, M.F. Toney. Adv. Funct. Mater. 25 (11) (2015) 1622-1637.
[4] I.L.C. Buurmans, B.M. Weckhuysen. Nat. Chem. 4 (2012) 873.
[5] J.-D. Grunwaldt, J.B. Wagner, R.E. Dunin-Borkowski. ChemCatChem 5 (1) (2013) 62-80.
[6] C.P. Grey, J.M. Tarascon. Nat. Mater. 16 (2016) 45.
[7] H. Wang, F. Wang. Curr. Opin. Chem. Eng. 13 (2016) 170-178.
[8] A. Vamvakeros, S.D.M. Jacques, V. Middelkoop, M. Di Michiel, C.K. Egan, I.Z. Ismagilov, G.B.M. Vaughan, F. Gallucci, M. van Sint Annaland, P.R. Shearing, R.J. Cernik, A.M. Beale. Chem. Commun. 51 (64) (2015) 12752-12755.
[9] P. Senecal, S.D.M. Jacques, M. Di Michiel, S.A.J. Kimber, A. Vamvakeros, Y. Odarchenko, I. Lezcano-Gonzalez, J. Paterson, E. Ferguson, A.M. Beale. ACS Catal. 7 (4) (2017) 2284-2293.
[10] A.M. Beale, S.D.M. Jacques, M. Di Michiel, J.F.W. Mosselmans, S.W.T. Price, P. Senecal, A. Vamvakeros, J. Paterson. Philos. T. Roy. Soc. A. 376 (2110) (2018).
[11] A. Vamvakeros, S.D.M. Jacques, M. Di Michiel, D. Matras, V. Middelkoop, I.Z. Ismagilov, E.V. Matus, V.V. Kuznetsov, J. Drnec, P. Senecal, A.M. Beale. Nat. Commun. 9 (1) (2018) 4751.
[12] D. Matras, S.D.M. Jacques, S. Poulston, N. Grosjean, C. Estruch Bosch, B. Rollins, J. Wright, M. Di Michiel, A. Vamvakeros, R.J. Cernik, A.M. Beale. J. Phys. Chem. C 123 (3) (2019) 1751-1760.
[13] T. Li, T.M.M. Heenan, M.F. Rabuni, B. Wang, N.M. Farandos, G.H. Kelsall, D. Matras, C. Tan, X. Lu, S.D.M. Jacques, D.J.L. Brett, P.R. Shearing, M. Di Michiel, A.M. Beale, A. Vamvakeros, K. Li. Nat. Commun. 10 (1) (2019) 1497.
[14] A. Vamvakeros, S.D.M. Jacques, M. Di Michiel, P. Senecal, V. Middelkoop, R.J. Cernik, A.M. Beale. Journal App. Crystallogr. 49 (2) (2016) 485-496.
[15] A. Vamvakeros, S.D.M. Jacques, M. Di Michiel, V. Middelkoop, C.K. Egan, R.J. Cernik, A.M. Beale. J. App. Crystallogr. 48 (6) (2015) 1943-1955.
[16] J. Kieffer, S. Petitdemange, T. Vincent. J. Synch. Rad. 25 (2) (2018) 612-617.
[17] A. Coelho. J. App. Crystallogr. 51 (1) (2018) 210-218.
[18] B. Christian Enger, R. Lødeng, A. Holmen. Appl. Catal. A- Gen. 346 (1) (2008) 1-27.
[19] D. Dissanayake, M.P. Rosynek, K.C.C. Kharas, J.H. Lunsford. J. Catal. 132 (1) (1991) 117-127.